
KernelNet: A Data-Dependent Kernel Parameterization for Deep Generative Modeling

Yufan Zhou

Department of CSE
University at Buffalo

Changyou Chen

Department of CSE
University at Buffalo

Jinhui Xu

Department of CSE
University at Buffalo

Abstract

Learning with kernels is an important concept in machine learning. Standard approaches for kernel methods often use predefined kernels that require careful selection of hyperparameters. To mitigate this burden, we propose in this paper a framework to construct and learn a data-dependent kernel based on random features and implicit spectral distributions parameterized by deep neural networks. The constructed network (called *KernelNet*) can be applied for deep generative modeling in various scenarios, including variants of the MMD-GAN and an implicit Variational Autoencoder (VAE), the two popular learning paradigms in deep generative models. Theoretically, we show that our proposed kernel indeed exists, and the induced Maximum Mean Discrepancy (MMD) endows the continuity in weak topology. Extensive experiments indicate that our proposed KernelNet consistently achieves better performance compared to related methods.

1 Introduction

Kernels are important tools in machine learning, and can be used in a wide range of applications. For example, support vector machine (SVM) (Schölkopf and Smola, 2002) can perform efficient non-linear classification task based on non-linear mappings through kernels; MMD-GAN (Li et al., 2017) can handle image generation task by utilizing Maximum Mean Discrepancy (MMD) (Gretton et al., 2012). Other kernel-based methods such as those by Yin and Zhou (2018); Feng et al. (2017) use kernels for estimating quantities like gradients. These models are built by either restricting the solution space to a Reproducing Kernel Hilbert Space (RKHS) induced by a kernel, or

adopting the MMD as the objective functions that require specified kernels in their MMDs.

A not-so-desirable issue of the aforementioned kernel-based methods, however, is the need of selecting appropriate kernels and hyper-parameters. Such selections are critical for obtaining good performance, and manual selection often leads to sub-optimal solutions. Some previous works have tried to mitigate this problem. For example, Gönen and Alpaydin (2011) suggests to learn a combination of some predefined kernels; Ong et al. (2004) proposes to relax the restriction of positive definiteness, which leads to a richer family of kernels. Alternatively, some other recent works focus on learning kernels based on random features (Rahimi and Recht, 2007; Bazavan et al., 2012; Wilson and Adams, 2013; Li et al., 2019) (see Section 3.1 for a more detailed description).

In this paper, we propose a new kernel-learning paradigm by formulating the kernel as an expectation w.r.t. learnable random features. These random features are sampled from an expressive distribution of the corresponding kernel in the spectral domain (which is called spectral distribution). Specifically, we parameterize the spectral distribution as a data-dependent distribution, meaning that it will depend on input data of the kernel function. The data-dependent distribution is represented by a deep neural network (DNN), which outputs samples following the distribution. We call the resulting network *KernelNet*, and the kernel corresponding to the data-dependent distribution a *data-dependent kernel*.

The work that is most related to ours is perhaps the one in Li et al. (2019). It models the spectral distribution as a data-independent distribution, and in some sense can be seen as a special case of our method. Due to the added data-dependent component in KernelNet, our method is thus more general and expressive. It could lead to performance improvement over the data-independent parameterization, as evidenced by our experiments.

Our proposed KernelNet can be readily applicable to a

number of existing models. As example, we show that it can be applied to two representative Deep Generative Models (DGMs): Generative Adversarial Network (GAN) (Goodfellow et al., 2014) and Variational Autoencoder (VAE) (Kingma and Welling, 2014; Rezende et al., 2014). Specifically, *i*) we apply our proposed kernel to several variants of MMD-GAN, including MMD-GAN (Li et al., 2017), scaled MMD-GAN (Arbel et al., 2018) and MMD-GAN with repulsive loss (Wang et al., 2018). We show that our proposed method leads to better performance and the induced MMD satisfies continuity in weak topology, which is an important property to ensure robustness of the optimization procedures. *ii*) We propose an implicit VAE model, where an MMD-regularizer is incorporated into the objective function of VAE. Our model is implicit in the sense that our posterior distribution is parameterized as an expressive distribution without a closed form, which is different from the typical Gaussian assumption in standard VAE and thus enables us to model a much more flexible latent space.

To summarize, our paper has the following contributions:

- We introduce the concept of data-dependent kernel, whose spectral distribution depends on the input pair of kernel. We demonstrate why data-dependent kernel exists, and propose a practical way to construct such a kernel.
- We show how to apply our proposed kernel to two popular models: GAN and VAE. We also prove that the MMD in our proposed GAN satisfies the continuity in weak topology.
- Extensive experiments suggest that our proposed kernel can lead to better performance compared to pre-defined kernel and previous representative kernel learning method (Li et al., 2019).

2 Preliminaries

We start by reviewing MMD-GAN and Info-VAE, two DGMs where our proposed data-dependent kernels apply.

2.1 MMD-GAN

GAN is one of the most popular and powerful generative models in deep learning. It consists of a generator and a discriminator. The generator generates samples by transforming a simple noise distribution to an implicit distribution \mathbb{Q} , where one can easily generate samples from this distribution, but the density function is unknown. The discriminator is trained to distinguish the true training data distribution \mathbb{P} and the implicit distribution \mathbb{Q} induced by the generator. The generator, on the other hand, is

trained to fool the discriminator. At the equilibrium, the generator should be able to generate samples that are distributed as the true data distribution \mathbb{P} .

MMD-GAN achieves this by minimizing the maximum mean discrepancy (MMD) between two probability measures, the data and model distributions. The MMD between two probability distributions \mathbb{P} and \mathbb{Q} is defined as:

$$\text{MMD}_k(\mathbb{P}, \mathbb{Q}) = \sup_{f: \|f\|_{\mathcal{H}} \leq 1} \mathbb{E}_{\mathbf{x} \sim \mathbb{P}}[f(\mathbf{x})] - \mathbb{E}_{\mathbf{y} \sim \mathbb{Q}}[f(\mathbf{y})]$$

where \mathcal{H} is a Reproducing Kernel Hilbert Space (RKHS) and f is a function in this RKHS.

For an RKHS induced by kernel k , MMD can be computed using the following equation:

$$\text{MMD}_k^2(\mathbb{P}, \mathbb{Q}) = \mathbb{E}_{\mathbf{x}, \mathbf{x}' \sim \mathbb{P}}[k(\mathbf{x}, \mathbf{x}')] - 2\mathbb{E}_{\mathbf{x} \sim \mathbb{P}, \mathbf{y} \sim \mathbb{Q}}[k(\mathbf{x}, \mathbf{y})] + \mathbb{E}_{\mathbf{y}, \mathbf{y}' \sim \mathbb{Q}}[k(\mathbf{y}, \mathbf{y}')].$$

For a characteristic kernel, $\text{MMD}_k(\mathbb{P}, \mathbb{Q}) = 0$ if and only if $\mathbb{P} = \mathbb{Q}$. Thus, MMD can be used as a way of measuring the similarity of distributions or as a training objective.

Li et al. (2017) propose to define the kernel as a composition of an injective function h_ϕ for feature extraction and a kernel function k for kernel evaluation, e.g., $k_\phi = k \circ h_\phi$. k_ϕ is also a valid kernel function by Shawe-Taylor and Cristianini (2004). For example, if k is the RBF kernel, $k_\phi(\mathbf{x}, \mathbf{y}) = \exp(-\|h_\phi(\mathbf{x}) - h_\phi(\mathbf{y})\|^2)$ is also a kernel.

Denote f_θ as a generator parameterized by θ . Let \mathbb{P} represent the training data distribution and \mathbb{Q} the implicit distribution induced by the generator. The objective of MMD-GAN is formulated as:

$$\min_{\theta} \max_{\phi} \text{MMD}_{k_\phi}^2(\mathbb{P}, \mathbb{Q}).$$

In MMD-GAN, both h_ϕ and f_θ are parameterized by neural networks, thus can be trained efficiently using gradient descent. Because of the min-max adversarial training, \mathbb{Q} will eventually match \mathbb{P} in theory.

However, MMD-GAN still suffers from training instability. It has been shown that better performance can be achieved by defining variants of MMD as objective functions.

Arbel et al. (2018) proposes to replace the objective function of MMD-GAN by the Scaled Maximum Mean Discrepancy (SMMD), which leads to the SMMD-GAN. The SMMD is defined as:

$$\text{SMMD}_{\phi, \lambda}(\mathbb{P}, \mathbb{Q}) := \sigma_{\phi, \lambda} \text{MMD}_{k_\phi}(\mathbb{P}, \mathbb{Q}),$$

where

$$\sigma_{\phi, \lambda} := \left\{ \lambda + \int k(\mathbf{x}, \mathbf{x}) d\mathbb{P}(\mathbf{x}) + \sum_{i=1}^d \int \frac{\partial^2 k(\mathbf{y}_1, \mathbf{y}_2)}{\partial \mathbf{y}_{1i} \partial \mathbf{y}_{2i}} \Big|_{(\mathbf{y}_1, \mathbf{y}_2) = (\mathbf{x}, \mathbf{x})} d\mathbb{P}(\mathbf{x}) \right\}^{-1/2},$$

and d is the dimensionality of the data; \mathbf{y}_i denotes the i^{th} element of \mathbf{y} ; λ is a hyper-parameter.

Wang et al. (2018) propose a repulsive loss function for the discriminator in MMD-GAN, which is defined as:

$$L_{\eta, \phi} = \eta \mathbb{E}_{\mathbf{x}, \mathbf{x}' \sim \mathbb{P}} [k_{\phi}(\mathbf{x}, \mathbf{x}')] - \mathbb{E}_{\mathbf{y}, \mathbf{y}' \sim \mathbb{Q}} [k_{\phi}(\mathbf{y}, \mathbf{y}')] - (\eta - 1) \mathbb{E}_{\mathbf{x} \sim \mathbb{P}, \mathbf{y} \sim \mathbb{Q}} [k_{\phi}(\mathbf{x}, \mathbf{y})].$$

Intuitively, the repulsive loss will explore the differences among data, leading to better performance in the data generation tasks.

One useful and important method in training GANs is spectral normalization (Miyato et al., 2018), which can control the Lipschitz constant of the injective function h_{ϕ} , leading to stable training and better performance. Spectral normalization normalizes the weight matrix \mathbf{W} by its spectral norm $\sigma(\mathbf{W})$:

$$\bar{\mathbf{W}} = \mathbf{W} / \sigma(\mathbf{W}), \text{ where } \sigma(\mathbf{W}) := \max_{\mathbf{h}: \|\mathbf{h}\| \neq 0} \|\mathbf{W} \mathbf{h}\| / \|\mathbf{h}\| = \max_{\|\mathbf{h}\| \leq 1} \|\mathbf{W} \mathbf{h}\|.$$

The Lipschitz constant of h_{ϕ} is thus bounded from above by 1. One can also set $\bar{\mathbf{W}} = c \mathbf{W} / \sigma(\mathbf{W})$, where c can either be a constant (Wang et al., 2018) or a learnable parameter (Arbel et al., 2018).

2.2 Info-VAE

VAE and its variants are another family of DGMs where latent spaces define the posterior distributions. Specifically, define a generative process for an observation $\mathbf{x} \in \mathbb{R}^D$, starting from the corresponding latent variable $\mathbf{z} \in \mathbb{R}^d$, as: $\mathbf{x} | \mathbf{z} \sim p_{\theta}(\mathbf{x} | \mathbf{z})$ with $\mathbf{z} \sim p(\mathbf{z})$, where $p(\mathbf{z})$ is called the prior distribution. Transformation from \mathbf{z} to \mathbf{x} is performed using a neural network parameterized by θ , which is called the decoder. For efficient inference of \mathbf{z} , VAE (Kingma and Welling, 2014) defines an inference network (or encoder) to generate \mathbf{z} from \mathbf{x} , with the corresponding distribution being $q_{\phi}(\mathbf{z} | \mathbf{x})$ parameterized by ϕ (also called the variational distribution or variational posterior distribution).

VAE is optimized by maximizing the Evidence Lower Bound (ELBO):

$$\max_{\phi, \theta} \mathbb{E}_{q_{\phi}(\mathbf{z} | \mathbf{x})} [\log p_{\theta}(\mathbf{x} | \mathbf{z})] - \text{KL}[q_{\phi}(\mathbf{z} | \mathbf{x}) || p(\mathbf{z})],$$

which can be understood as simultaneously reconstructing the observations and minimizing the Kullback-Leibler (KL) divergence between prior and posterior distributions.

Info-VAE (Zhao et al., 2017) is a generalization of VAE by introducing an information-theoretic regularizer into the VAE framework. The objective of Info-VAE is:

$$\max_{\phi, \theta} - \mathbb{E}_{q_{\phi}(\mathbf{z})} \{ \text{KL}[q_{\phi}(\mathbf{x} | \mathbf{z}) || p_{\theta}(\mathbf{x} | \mathbf{z})] \} + \alpha \mathbf{I}_{q_{\phi}}(\mathbf{x}, \mathbf{z}) - \lambda \text{KL}[q_{\phi}(\mathbf{z}) || p(\mathbf{z})], \quad (1)$$

where α and λ are hyper-parameters, and $\mathbf{I}_{q_{\phi}}(\mathbf{x}, \mathbf{z})$ is the mutual information between \mathbf{x} and \mathbf{z} defined as:

$$\mathbf{I}_{q_{\phi}}(\mathbf{x}, \mathbf{z}) = \mathbb{E}_{q(\mathbf{x})} \{ \text{KL}[q_{\phi}(\mathbf{z} | \mathbf{x}) || q_{\phi}(\mathbf{z})] \}.$$

Note that both KL and MMD describe difference between distributions. Thus in our approach, we propose to replace the mutual information term with an MMD regularizer. Furthermore, our model considers an implicit setting where q_{ϕ} is defined as an implicit distribution, making our model more expressive. Details will be presented in the later sections.

3 KernelNet for Learning Deep Generative Models

3.1 The Proposed KernelNet

To alleviate the difficulties with pre-defined kernels such as hyperparameter selection, we propose KernelNet, a principled way to parameterize a kernel with a DNN. Our method improves the recent work (Li et al., 2019) by making the kernel data-dependent and applying it to different DGMs.

We start with a classic result on positive definite functions (Rudin, 1994), stated in Lemma 1.

Lemma 1 (Rudin (1994)) *A continuous function $\kappa(\mathbf{z})$ in \mathbb{R}^d is positive definite if and only if it is the Fourier transform of a non-negative measure.*

Let $\zeta_{\omega}(\mathbf{z}) = e^{j\omega^{\top} \mathbf{z}}$. By Lemma 1 and (Rahimi and Recht, 2007), a kernel such that $\kappa(\mathbf{z}_1, \mathbf{z}_2) = \tilde{\kappa}(\mathbf{z}_1 - \mathbf{z}_2)$ can be represented as:

$$\begin{aligned} \kappa(\mathbf{z}_1, \mathbf{z}_2) &= \int_{\mathbb{R}^d} p(\omega) e^{j\omega^{\top} (\mathbf{z}_1 - \mathbf{z}_2)} d\omega \\ &= \mathbb{E}_{\omega} [\zeta_{\omega}(\mathbf{z}_1) \zeta_{\omega}(\mathbf{z}_2)^*], \end{aligned} \quad (2)$$

where j is an indeterminate satisfying $j^2 = -1$, and “*” denotes the conjugate transpose. The kernel representation (2) directly allows us to construct an unbiased estimator for $\kappa(\cdot, \cdot)$ by introducing any valid distribution $p(\omega)$ for the augmented variable ω , called the *spectral*

distribution. In the following, we first reformulate (2) into two equivalent forms for the purposes of analysis and algorithm design, respectively. Because the probability density function and kernel function are real-valued, by Euler’s formula, we can rewrite the kernel as following.

Proposition 2 *Let ω be drawn from some spectral distribution $p(\omega)$, and b be drawn uniformly from $[0, 2\pi]$. The real-valued kernel in (2) can be reformulated into the following two forms:*

$$\kappa(\mathbf{z}_1, \mathbf{z}_2) = \mathbb{E}_{\omega \sim p(\omega)} \{ \cos[\omega^\top (\mathbf{z}_1 - \mathbf{z}_2)] \} \quad (3)$$

$$= \mathbb{E}_{\omega, b} [2 \cos(\omega^\top \mathbf{z}_1 + b) \cos(\omega^\top \mathbf{z}_2 + b)] \quad (4)$$

where $\omega \sim p(\omega)$, $b \sim \mathcal{U}[0, 2\pi]$.

Detailed derivations can be found in Appendix A. In the above two representation, (3) is more convenient for theoretical analysis, and (4) is found more stable in algorithmic implementation.

To enhance the expressive power, we can make the distribution $p(\omega)$ complex enough and learnable by parameterizing it with a DNN that induces an implicit distribution. Specifically, we rewrite $p(\omega)$ as $p_{\psi_1}(\omega)$ with parameter ψ_1 . A sample ω from p_{ψ_1} is modeled as the following generating process:

$$\omega_{\psi_1} = g_{\psi_1}(\epsilon), \quad \epsilon \sim \mathcal{N}(\mathbf{0}, \mathbf{I}), \quad (5)$$

where $g_{\psi_1}(\epsilon)$ denotes the output of a DNN parameterized by ψ_1 with the input ϵ drawn from some simple distributions like standard Gaussian or uniform distributions.

Extension to data-dependent kernels Although the above kernel parameterization is flexible to represent a rich family of implicit spectral distributions, it can be further extended by introducing a data-dependent spectral distribution. By data-dependent spectral distribution, we mean that there are some kernels satisfying (2), whose spectral distributions $p(\omega)$ depend on the data pair $(\mathbf{z}_1, \mathbf{z}_2)$, *i.e.*, there exists a $p(\omega | \mathbf{z}_1, \mathbf{z}_2)$ for each pair $(\mathbf{z}_1, \mathbf{z}_2)$.

We use the term data-dependent because it allows us to construct more flexible kernels. For example: 1) For a given input pair $(\mathbf{z}_1, \mathbf{z}_2)$, the spectral distributions and the kernel values $\kappa(\mathbf{z}_1, \mathbf{z}_2)$ depend on the input pair $(\mathbf{z}_1, \mathbf{z}_2)$. Thus $\mathbf{z}_1 - \mathbf{z}_2 = \mathbf{z}_3 - \mathbf{z}_4$ does not necessarily imply $\kappa(\mathbf{z}_1, \mathbf{z}_2) = \kappa(\mathbf{z}_3, \mathbf{z}_4)$; 2) The marginal distribution $p(\omega)$ depends on specific datasets, which could induce different formulas on different datasets.

One example of such a kernel is symmetric positive definite kernel defined on a Riemannian manifold $\mathcal{M} \subset R^d$, whose value depends on the geodesic distance between two points rather than the standard Euclidean distance.

Constructing a data-dependent KernelNet To construct a data-dependent KernelNet, we extend (5) to the following process:

$$\omega_{\psi_2, \mathbf{z}_1, \mathbf{z}_2} = g_{\psi_2}(\epsilon, \mathbf{z}_1, \mathbf{z}_2) \text{ with } \epsilon \sim \mathcal{N}(\mathbf{0}, \mathbf{I}).$$

Note that such an implicit construction requires multiple noise samples to approximate the distribution of $\omega_{\psi_2, \mathbf{z}_1, \mathbf{z}_2}$ for every $(\mathbf{z}_1, \mathbf{z}_2)$ pair, which could be time consuming when the mini-batch sizes are large. To tackle this issue, we propose to decompose a kernel into two components: a data-dependent component and a data-independent component, and utilize the reparameterization trick in the data-dependent component. Note that such a decomposition still guarantees the implicitity and data-dependency of the overall kernel, and thus will not lose generalization.

For the data-dependent component, given an input pair $(\mathbf{z}_1, \mathbf{z}_2)$, we first define a data-dependent sampling process as following:

$$\omega'_{\psi_2, \mathbf{z}_1, \mathbf{z}_2} = \boldsymbol{\mu}_{\psi_2, \mathbf{z}_1, \mathbf{z}_2} + \epsilon \odot \boldsymbol{\sigma}_{\psi_2, \mathbf{z}_1, \mathbf{z}_2}, \quad \epsilon \sim \mathcal{N}(\mathbf{0}, \mathbf{I}), \quad (6)$$

where $\boldsymbol{\mu}_{\psi_2, \mathbf{z}_1, \mathbf{z}_2}$ and $\boldsymbol{\sigma}_{\psi_2, \mathbf{z}_1, \mathbf{z}_2}$ are outputs from a DNN parameterized by ψ_2 ; \odot denotes the element-wise multiplication. Since $\omega'_{\psi_2, \mathbf{z}_1, \mathbf{z}_2}$ depends on input pair $(\mathbf{z}_1, \mathbf{z}_2)$, its probability distribution is actually data-dependent.

However, this sampling process may lead to an asymmetric kernel, thus we further set

$$\omega_{\psi_2, \mathbf{z}_1, \mathbf{z}_2} = (\omega'_{\psi_2, \mathbf{z}_1, \mathbf{z}_2} + \omega'_{\psi_2, \mathbf{z}_2, \mathbf{z}_1})/2,$$

and use $\omega_{\psi_2, \mathbf{z}_1, \mathbf{z}_2}$ as random features for a kernel.

For the data-independent component, we adopt the implicit representation defined in (5). Consequently, the overall KernelNet is constructed as:

$$\kappa_{\psi}(\mathbf{z}_1, \mathbf{z}_2) \triangleq \kappa_{\psi_1}(\mathbf{z}_1, \mathbf{z}_2) + \kappa_{\psi_2}(\mathbf{z}_1, \mathbf{z}_2), \text{ where} \quad (7)$$

$$\kappa_{\psi_1}(\mathbf{z}_1, \mathbf{z}_2) = \mathbb{E}_{\omega_{\psi_1}, b} \left[2 \cos(\omega_{\psi_1}^\top \mathbf{z}_1 + b) \cos(\omega_{\psi_1}^\top \mathbf{z}_2 + b) \right],$$

$$\kappa_{\psi_2}(\mathbf{z}_1, \mathbf{z}_2) = \mathbb{E}_{\omega_{\psi_2, \mathbf{z}_1, \mathbf{z}_2}, b} \left[2 \cos(\omega_{\psi_2, \mathbf{z}_1, \mathbf{z}_2}^\top \mathbf{z}_1 + b) \right. \\ \left. \times \cos(\omega_{\psi_2, \mathbf{z}_1, \mathbf{z}_2}^\top \mathbf{z}_2 + b) \right].$$

The network structure is illustrated in Figure 1. In implementation, expectations are approximated by samples, *e.g.*:

$$\mathbb{E}_{\omega_{\psi_1}, b} \left[2 \cos(\omega_{\psi_1}^\top \mathbf{z}_1 + b) \cos(\omega_{\psi_1}^\top \mathbf{z}_2 + b) \right] \\ \approx \frac{2}{N} \sum_{i=1}^N \cos(\omega_{\psi_1 i}^\top \mathbf{z}_1 + b_i) \cos(\omega_{\psi_1 i}^\top \mathbf{z}_2 + b_i),$$

where all $\omega_{\psi_1 i}$ ’s are samples from the spectral distributions $p(\omega_{\psi_1})$ through (5). In addition, b_i ’s are drawn from $p(b) = \mathcal{U}[0, 2\pi]$.

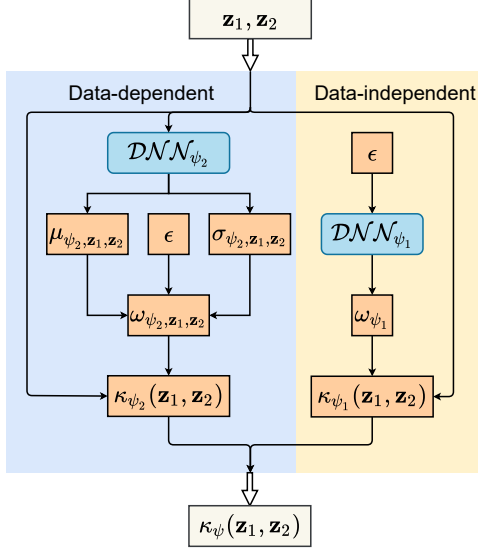


Figure 1: Structure of the proposed KernelNet, where $\epsilon \sim \mathcal{N}(\mathbf{0}, \mathbf{I})$.

Since the construction is implicit with no stochastic intermediate nodes, standard back-propagation can be applied for efficient end-to-end training. Lemma 3 below indicates the summation of two kernels is still a kernel, guaranteeing that the output of the KernelNet (7) is still a legitimate kernel.

Lemma 3 (Shawe-Taylor and Cristianini (2004)) *Let $\kappa_1(\mathbf{z}_1, \mathbf{z}_2)$ and $\kappa_2(\mathbf{z}_1, \mathbf{z}_2)$ be two kernels over $R^d \times R^d$, then $\kappa'(\mathbf{z}_1, \mathbf{z}_2) \triangleq \kappa_1(\mathbf{z}_1, \mathbf{z}_2) + \kappa_2(\mathbf{z}_1, \mathbf{z}_2)$ is also a kernel.*

It is worth noting that the kernel reduces to the one in Li et al. (2019) when removing the data-dependent component. We will show in the experiments that the data-dependent component indeed plays an important role, and can lead to performance improvement in different tasks.

3.2 KernelNet for MMD-GAN

In this section, we incorporate the proposed KernelNet into learning the MMD-GAN model. We seek to develop an algorithm to jointly optimize both the KernelNet and the MMD-GAN model. A straightforward way is to replace the standard kernel in MMD-GAN with the proposed data-dependent kernel (7). However, as the standard MMD-GAN fails to satisfy *continuity in weak topology* (Arbel et al., 2018), it is unclear whether the variant with our KernelNet would satisfy the property. To this end, we first define *continuity in weak topology*.

Continuity in weak topology (Arbel et al., 2018) $\text{MMD}_k(\mathbb{Q}, \mathbb{P})$ is said to endow continuity in weak

topology if $\mathbb{Q} \xrightarrow{D} \mathbb{P}$ implies $\text{MMD}_k(\mathbb{Q}, \mathbb{P}) \rightarrow 0$, where \xrightarrow{D} means convergence in distribution.

Continuity in weak topology in MMD-GAN is important because it makes a loss provide better signal to the generator as \mathbb{Q} approaches \mathbb{P} , without suffering from sudden jump as in the Jensen-Shannon (JS) divergence or KL divergence (e.g. Example 1 in Arjovsky et al. (2017)). MMD in MMD-GAN without constrain may not be continuous in the weak topology, leading to training instability and poor performance. To alleviate this problem, a number of methods have been introduced, e.g., through weight-clipping (Li et al., 2017), gradient penalty (Gulrajani et al., 2017), spectral normalization (Miyato et al., 2018), and adopting a scaled objective (SMMD-GAN) (Arbel et al., 2018). Fortunately, we can prove that adopting our KernelNet in MMD-GAN can lead to continuity in weak topology.

Proposition 4 *By parameterizing the kernel with our KernelNet $\kappa_{\psi}(\mathbf{z}_1, \mathbf{z}_2) = \kappa_{\psi_1}(\mathbf{z}_1, \mathbf{z}_2) + \kappa_{\psi_2}(\mathbf{z}_1, \mathbf{z}_2)$, $\text{MMD}_{\phi, \psi}(\mathbb{P}, \mathbb{Q})$ is continuous in the weak topology if the following are satisfied:*

$$\begin{aligned} \mathbb{E}_{\omega_{\psi_1}} [\|\omega_{\psi_1}\|^2] < \infty, \quad \mathbb{E}_{\omega_{\psi_2, \mathbf{z}_1, \mathbf{z}_2}} [\|\omega_{\psi_2, \mathbf{z}_1, \mathbf{z}_2}\|^2] < \infty, \\ \mathbb{E}_{\omega_{\psi_2, \mathbf{z}_1, \mathbf{z}_2}} \left[\left\| \frac{\partial \omega_{\psi_2, \mathbf{z}_1, \mathbf{z}_2}}{\partial \mathbf{z}_1} - \frac{\partial \omega_{\psi_2, \mathbf{z}_1, \mathbf{z}_2}}{\partial \mathbf{z}_2} \right\|_{\mathcal{F}} \right] < \infty, \\ \sup_{\phi \in \Phi} \|h_{\phi}\|_{Lip} < \infty \end{aligned} \quad (8)$$

where $\|\cdot\|_{\mathcal{F}}$ denotes the Frobenius norm of a matrix, h_{ϕ} is the injective function in MMD-GAN, i.e., $\mathbf{z} = h_{\phi}(\mathbf{x})$, and $\|h_{\phi}\|_{Lip}$ denotes its Lipschitz constant.

The proof can be found in Appendix B. Based on Proposition 4, we propose several variants of the MMD-GAN model, respectively corresponding to the MMD-GAN (Li et al., 2017), SMMD-GAN (Arbel et al., 2018) and MMD-GAN with repulsive loss (denoted as Rep-GAN) (Wang et al., 2018), by incorporating the conditions in Proposition 4 into the objective functions.

MMD-GAN with the KernelNet By adopting spectral normalization and the method of Lagrange multipliers to regularize the conditions in Proposition 4, we propose SN-MMD-GAN-DK. Note that $\sup_{\phi \in \Phi} \|h_{\phi}\|_{Lip} < \infty$ is satisfied because of the spectral normalization operation, which normalizes the weight matrix during the training process. The objective of generator and discriminator are defined as:

$$\begin{aligned} \min_{\theta} \text{MMD}_{\phi, \psi}^2(\mathbb{P}, \mathbb{Q}) + \alpha_1 \Omega(\theta, \phi, \psi), \text{ and} \\ \min_{\phi, \psi} -\text{MMD}_{\phi, \psi}^2(\mathbb{P}, \mathbb{Q}) + \alpha_2 \Omega(\theta, \phi, \psi), \text{ where} \end{aligned} \quad (9)$$

$$\begin{aligned} \Omega(\boldsymbol{\theta}, \boldsymbol{\phi}, \boldsymbol{\psi}) &\triangleq \mathbb{E}_{\boldsymbol{\omega}_{\psi_1}} [\|\boldsymbol{\omega}_{\psi_1}\|^2] + \mathbb{E}_{\boldsymbol{\omega}_{\psi_2, \mathbf{z}_1, \mathbf{z}_2}} [\|\boldsymbol{\omega}_{\psi_2, \mathbf{z}_1, \mathbf{z}_2}\|^2] \\ &+ \left\| \frac{\partial \boldsymbol{\omega}_{\psi_2, \mathbf{z}_1, \mathbf{z}_2}}{\partial \mathbf{z}_1} - \frac{\partial \boldsymbol{\omega}_{\psi_2, \mathbf{z}_1, \mathbf{z}_2}}{\partial \mathbf{z}_2} \right\|_{\mathcal{F}}. \end{aligned} \quad (10)$$

Scaled MMD-GAN with the KernelNet Similarly, based on the SMMD-GAN model by Arbel et al. (2018), we propose our variant SN-SMMD-GAN-DK by incorporating the conditions in Proposition 4 into the SMMD framework.

Proposition 5 *With the proposed data-dependent KernelNet (7), the SMMD-DK framework can be formulated and simplified as:*

$$\text{SMMD-DK}_{\boldsymbol{\phi}, \boldsymbol{\psi}, \lambda}(\mathbb{P}, \mathbb{Q}) := \sigma_{\boldsymbol{\phi}, \boldsymbol{\psi}, \lambda} \text{MMD}_{\boldsymbol{\phi}, \boldsymbol{\psi}}(\mathbb{P}, \mathbb{Q}),$$

where

$$\begin{aligned} \sigma_{\boldsymbol{\phi}, \boldsymbol{\psi}, \lambda} &:= \left\{ \lambda + 1 + \mathbb{E}_{\mathbf{x} \sim \mathbb{P}} \left\{ \mathbb{E}_{\boldsymbol{\omega}_{\psi_2, \mathbf{z}, \mathbf{z}}} [\|\boldsymbol{\omega}_{\psi_2, \mathbf{z}, \mathbf{z}}\|^2] \|\nabla h_{\boldsymbol{\phi}}(\mathbf{x})\|_{\mathcal{F}} \right\} \right. \\ &\quad \left. + \mathbb{E}_{\mathbf{x} \sim \mathbb{P}} \left\{ \mathbb{E}_{\boldsymbol{\omega}_{\psi_1}} [\|\boldsymbol{\omega}_{\psi_1}\|^2] \|\nabla h_{\boldsymbol{\phi}}(\mathbf{x})\|_{\mathcal{F}} \right\} \right\}^{-1/2}, \end{aligned}$$

and $\mathbf{z} = h_{\boldsymbol{\phi}}(\mathbf{x})$.

The derivation can be found in Appendix C. Consequently, by incorporating the conditions in Proposition 4, the objectives for generator and discriminator in SN-SMMD-GAN-DK are defined as:

$$\begin{aligned} \min_{\boldsymbol{\theta}} \text{SMMD-DK}_{\boldsymbol{\phi}, \boldsymbol{\psi}, \lambda}^2(\mathbb{P}, \mathbb{Q}) + \alpha_1 \Omega(\boldsymbol{\theta}, \boldsymbol{\phi}, \boldsymbol{\psi}), \\ \min_{\boldsymbol{\phi}, \boldsymbol{\psi}} -\text{SMMD-DK}_{\boldsymbol{\phi}, \boldsymbol{\psi}, \lambda}^2(\mathbb{P}, \mathbb{Q}) + \alpha_2 \Omega(\boldsymbol{\theta}, \boldsymbol{\phi}, \boldsymbol{\psi}), \end{aligned} \quad (11)$$

where $\Omega(\boldsymbol{\theta}, \boldsymbol{\phi}, \boldsymbol{\psi})$ is defined as (10).

In practice, we choose λ and scale the original SMMD-DK objective so that the ‘‘SMMD-DK²’’ in (11) is replaced by the following:

$$\widehat{\text{SMMD-DK}}_{\boldsymbol{\psi}, \boldsymbol{\phi}, \zeta}^2(\mathbb{P}, \mathbb{Q}) = \delta_{\boldsymbol{\phi}, \boldsymbol{\psi}, \zeta} \text{MMD}_{\kappa_{\boldsymbol{\psi}}}^2(\mathbb{P}, \mathbb{Q}) \quad (12)$$

where

$$\begin{aligned} \delta_{\boldsymbol{\phi}, \boldsymbol{\psi}, \zeta} &:= \left\{ 1 + \zeta \mathbb{E}_{\mathbf{x} \sim \mathbb{P}} \left\{ \mathbb{E}_{\boldsymbol{\omega}_{\psi_2, \mathbf{z}, \mathbf{z}}} [\|\boldsymbol{\omega}_{\psi_2, \mathbf{z}, \mathbf{z}}\|^2] \|\nabla h_{\boldsymbol{\phi}}(\mathbf{x})\|_{\mathcal{F}} \right\} \right. \\ &\quad \left. + \mathbb{E}_{\mathbf{x} \sim \mathbb{P}} \left\{ \mathbb{E}_{\boldsymbol{\omega}_{\psi_1}} [\|\boldsymbol{\omega}_{\psi_1}\|^2] \|\nabla h_{\boldsymbol{\phi}}(\mathbf{x})\|_{\mathcal{F}} \right\} \right\}^{-1}. \end{aligned}$$

Repulsive loss with the KernelNet By incorporating KernelNet into the repulsive loss, we further propose Rep-GAN-DK. According to Proposition 4, the objective

functions for generator and discriminator in Rep-GAN-DK are defined as:

$$\begin{aligned} \min_{\boldsymbol{\theta}} \text{MMD}_{\boldsymbol{\phi}, \boldsymbol{\psi}}^2(\mathbb{P}, \mathbb{Q}) + \alpha_1 \Omega(\boldsymbol{\theta}, \boldsymbol{\phi}, \boldsymbol{\psi}), \text{ and} \\ \min_{\boldsymbol{\phi}, \boldsymbol{\psi}} L_{\eta, \boldsymbol{\phi}, \boldsymbol{\psi}} + \alpha_2 \Omega(\boldsymbol{\theta}, \boldsymbol{\phi}, \boldsymbol{\psi}), \end{aligned} \quad (13)$$

where

$$\begin{aligned} L_{\eta, \boldsymbol{\phi}, \boldsymbol{\psi}} &= \eta \mathbb{E}_{\mathbf{x}, \mathbf{x}' \sim \mathbb{P}} [k_{\boldsymbol{\phi}, \boldsymbol{\psi}}(\mathbf{x}, \mathbf{x}')] - \mathbb{E}_{\mathbf{y}, \mathbf{y}' \sim \mathbb{Q}} [k_{\boldsymbol{\phi}, \boldsymbol{\psi}}(\mathbf{y}, \mathbf{y}')] \\ &\quad - (\eta - 1) \mathbb{E}_{\mathbf{x} \sim \mathbb{P}, \mathbf{y} \sim \mathbb{Q}} [k_{\boldsymbol{\phi}, \boldsymbol{\psi}}(\mathbf{x}, \mathbf{y})], \end{aligned} \quad (14)$$

$\Omega(\boldsymbol{\theta}, \boldsymbol{\phi}, \boldsymbol{\psi})$ is defined as (10), η is a hyper-parameter. One can find that when $\eta = -1$, (13) will reduce to the standard MMD case (9).

3.3 KernelNet for Implicit Info-VAE

In this section, we describe how to incorporate our KernelNet into the Info-VAE framework. First, to increase the power of Info-VAE, we adopt an implicit encoder setting. That is, instead of adopting a particular posterior distribution family such as Gaussian for the encoder, we construct a complex implicit distribution by adding random noise at each layer of the encoder (including input data) and removing the reparameterization trick.

One problem with such a method is the need of evaluating the density of the implicit encoder distribution for model training, as seen in the objective (1). To deal with this issue, we adopt the Stein gradient estimator (SGE) (Li and Turner, 2018) to approximate the gradient of the log-density.

Another problem is the difficulty of computing mutual information (MI). MI between two distributions is easy to be handled only in certain situations, e.g. both of them are Gaussian. In the implicit VAE setting, one has to design some non-trivial methods to deal with the intractability of the mutual information. In our work, we propose to replacing the mutual information with MMD. The logic is quite straightforward because both MMD and MI can be reconsidered as distance measures of two distributions. MMD is much easier to be dealt with, because it can be computed based on samples regardless of how complex the distributions are. Consequently, we apply our proposed KernelNet to the computation of MMD, which leads to the following objective:

$$\begin{aligned} \max_{\boldsymbol{\phi}, \boldsymbol{\theta}, \boldsymbol{\psi}} -\lambda \text{KL}[q_{\boldsymbol{\phi}}(\mathbf{z}) \| p(\mathbf{z})] - \mathbb{E}_{q_{\boldsymbol{\phi}}(\mathbf{z})} \{ \text{KL}[q_{\boldsymbol{\phi}}(\mathbf{x} | \mathbf{z}) \| p_{\boldsymbol{\theta}}(\mathbf{x} | \mathbf{z})] \} \\ + \alpha \mathbb{E}_{q(\mathbf{x})} \{ \text{MMD}_{\boldsymbol{\psi}}[q_{\boldsymbol{\phi}}(\mathbf{z} | \mathbf{x}), q_{\boldsymbol{\phi}}(\mathbf{z})] \}, \end{aligned}$$

with hyper-parameter λ and α . The objective can be further reformulated as:

$$\begin{aligned} \max_{\boldsymbol{\phi}, \boldsymbol{\theta}, \boldsymbol{\psi}} \mathbb{E}_{q(\mathbf{x})} \mathbb{E}_{q_{\boldsymbol{\phi}}(\mathbf{z} | \mathbf{x})} [\log p_{\boldsymbol{\theta}}(\mathbf{x} | \mathbf{z})] - \mathbb{E}_{q(\mathbf{x})} \{ \text{KL}[q_{\boldsymbol{\phi}}(\mathbf{z} | \mathbf{x}) \| p(\mathbf{z})] \} \\ - \mathbb{E}_{q(\mathbf{x})} (\log q(\mathbf{x})) - (\lambda - 1) \text{KL}[q_{\boldsymbol{\phi}}(\mathbf{z}) \| p(\mathbf{z})] \\ + \alpha \mathbb{E}_{q(\mathbf{x})} \{ \text{MMD}_{\boldsymbol{\psi}}[q_{\boldsymbol{\phi}}(\mathbf{z} | \mathbf{x}), q_{\boldsymbol{\phi}}(\mathbf{z})] \}. \end{aligned} \quad (15)$$

Table 1: Comparison between IKL and our KernelNet

	CIFAR-10	
	FID (\downarrow)	IS (\uparrow)
SN-MMD-GAN	31.5 ± 0.2	6.9 ± 0.1
SN-MMD-GAN-IKL	30.4 ± 0.1	6.9 ± 0.1
SN-MMD-GAN-DK (OURS)	27.8 ± 0.1	7.2 ± 0.1
SN-SMMD-GAN	25.0 ± 0.3	7.3 ± 0.1
SN-SMMD-GAN-IKL	26.4 ± 0.1	7.3 ± 0.1
SN-SMMD-GAN-DK (OURS)	24.3 ± 0.1	7.4 ± 0.1
REP-GAN	16.7	8.0
REP-GAN-IKL	16.3 ± 0.1	8.0 ± 0.1
REP-GAN-DK (OURS)	15.2 ± 0.1	8.1 ± 0.1

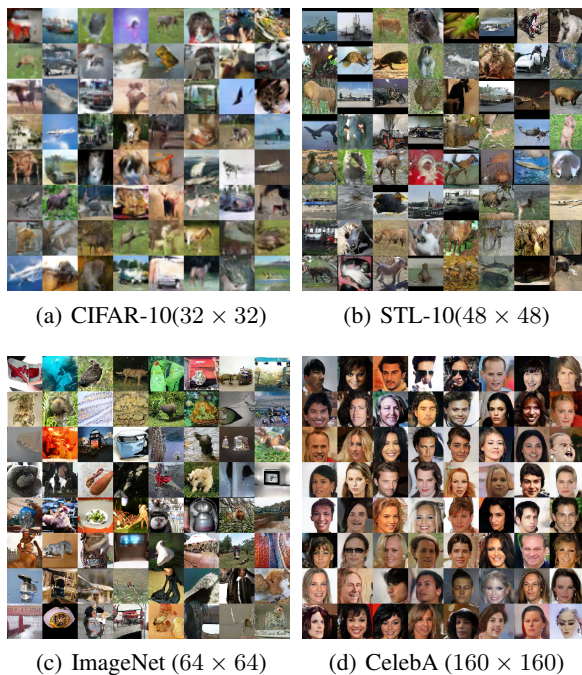


Figure 2: Generated images of SN-SMMD-GAN-DK.

Note that $\mathbb{E}_{q(\mathbf{x})}(\log q(\mathbf{x}))$ is independent of the model, and thus can be discarded in optimization. Our proposed model is more general than VAE: when $\lambda = 1$ and $\alpha = 0$, (15) reduces to the objective of vanilla VAE.

4 Experiments

We conduct experiments to test the performance of our proposed KernelNet applied to variants of MMD-GAN and implicit VAE, and compare them with related methods, including MMD and non-MMD based GANs, semi-implicit and implicit VAE models. Our experiments are implemented using Tensorflow on a Nvidia Titan Xp GPU, all the code will be available online.

4.1 MMD-GAN

We evaluated our MMD-GAN variants on four datasets: CIFAR-10, STL-10, ImageNet and CelebA. Following Arbel et al. (2018) and Wang et al. (2018), we scale training images from these datasets to the resolution of 32×32 , 48×48 , 64×64 and 160×160 respectively.

We compare our models with WGAN-GP (Gulrajani et al., 2017), MMD-GAN (Li et al., 2017), SN-GAN (Miyato et al., 2018), SMMD-GAN, SN-SMMD-GAN (Arbel et al., 2018), Rep-GAN (Wang et al., 2018), CR-GAN (Zhang et al., 2020).

For a fair comparison, all the models are evaluated under the same architecture on each dataset. Our model architectures follow Arbel et al. (2018). For CIFAR-10 and STL-10, we use an architecture with a 7-layer convolutional neural network (CNN) as the discriminator and a 4-layer CNN as the generator. For CelebA, we use a 5-layer CNN discriminator and a 10-layer ResNet generator. For ImageNet, our generator and discriminator are both 10-layer ResNets. The output dimension of discriminator is set to be 1 for all the models, except that it is set to 16 when repulsive loss is used. Inputs of the generator are sampled from a uniform distribution $\mathcal{U}[-1, 1]^{128}$. We use two 3-layer fully-connected neural networks to parameterize ω_{ψ_1} and $\omega_{\psi_2, z_1, z_2}$. For each neural network, there are 16 neurons in every hidden layer when the discriminator’s output dimension is 1, and 64 neurons when the discriminator’s output dimension is 16.

Spectral normalization (Miyato et al., 2018) is used in most of the models except WGAN-GP and SMMD-GAN, spectral parameterization (Arbel et al., 2018) is used in SN-SMMD-GAN-DK. Note that in Rep-GAN-DK, we scale the weight after spectral normalization by a constant chosen from $\{0.5, 1, 2\}$ based on hyper-parameter tuning, which is similar to Wang et al. (2018).

Adam optimizer (Kingma and Ba, 2015) with batch size of 64 is used in all the experiments. Learning rates of generator and discriminator are selected from $\{0.0001, 0.0002\}$. At every update step, 1024 samples of ω_{ψ_1} and ω_{ψ_2} are used to compute the values of the kernel function. We set $\alpha_1 = 0$, $\alpha_2 = 5$ in (9), $\alpha_1 = 0$, $\alpha_2 = 0.1$ in (11) and $\alpha_1 = 0$, $\alpha_2 = 0.01$ in (13) respectively.

In SN-MMD-GAN-DK and SN-SMMD-GAN-DK, we update discriminator and KernelNet 5 steps for every generator update. ζ in (12) is selected from $\{1, 2, 5\}$. Ratio of learning rate of KernelNet to learning rate of generator is selected from $\{0.01, 0.005\}$. The hyper-parameters of Adam optimizer are set to be $\beta_1 = 0.5$, $\beta_2 = 0.9$. Models are trained for 150,000 generator update steps for CIFAR-10, STL-10 and CelebA, 200,000 generator update steps for ImageNet.

Table 2: Results of image generation.

	CIFAR-10		STL-10		CELEBA		IMAGENET	
	FID (\downarrow)	IS (\uparrow)	FID (\downarrow)	IS (\uparrow)	FID (\downarrow)	IS (\uparrow)	FID (\downarrow)	IS (\uparrow)
WGAN-GP	31.1 \pm 0.2	6.9 \pm 0.2	55.1	8.4 \pm 0.1	29.2 \pm 0.2	2.7 \pm 0.1	65.7 \pm 0.3	7.5 \pm 0.1
SN-GAN	25.5	7.6 \pm 0.1	43.2	8.8 \pm 0.1	22.6 \pm 0.1	2.7 \pm 0.1	47.5 \pm 0.1	11.2 \pm 0.1
SMMD-GAN	31.5 \pm 0.4	7.0 \pm 0.1	43.7 \pm 0.2	8.4 \pm 0.1	18.4 \pm 0.2	2.7 \pm 0.1	38.4 \pm 0.3	10.7 \pm 0.2
SN-SMMD-GAN	25.0 \pm 0.3	7.3 \pm 0.1	40.6 \pm 0.1	8.5 \pm 0.1	12.4 \pm 0.2	2.8 \pm 0.1	36.6 \pm 0.2	10.9 \pm 0.1
SN-SMMD-GAN-DK (OURS)	24.3 \pm 0.1	7.4 \pm 0.1	40.0 \pm 0.1	8.5 \pm 0.1	11.3 \pm 0.1	2.9 \pm 0.1	35.7 \pm 0.3	11.2 \pm 0.2
CR-GAN	18.7	7.9	–	–	–	–	–	–
REP-GAN	16.7	8.0	36.7	9.4	16.8 \pm 0.1	2.9 \pm 0.1	31.0 \pm 0.1	11.5 \pm 0.1
REP-GAN-DK (OURS)	15.2 \pm 0.1	8.1 \pm 0.1	34.9 \pm 0.1	9.3 \pm 0.1	16.1 \pm 0.1	2.9 \pm 0.1	30.5 \pm 0.1	11.7 \pm 0.1

In Rep-GAN-DK, we update the discriminator and KernelNet one step for every generator update, the learning rate of KernelNet is set to be half of the generator. The hyperparameters of Adam optimizer are set to be $\beta_1 = 0.5$, $\beta_2 = 0.999$. η in (14) is selected from $\{0, 0.5, 1\}$. Models are trained for 200,000 generator update steps for CIFAR-10 and CelebA, 300,000 generator update steps for STL-10 and ImageNet.

We report the standard Fréchet Inception Distance (FID) (Heusel et al., 2017) and Inception Score (IS) (Salimans et al., 2016). They are computed using 100,000 samples on CIFAR-10, Stl-10 and ImageNet datasets, while 50,000 samples are used on CelebA due to the GPU memory limitation. During the training process, we decrease the learning rate based on the relative KID test (Bounliphone et al., 2016). The frequency of decreasing the learning rate are based on hyper-parameter tuning.

To illustrate the effectiveness of our data-dependent component, we first compare with models using kernels without the data-dependent component, which is the same as the IKL method proposed by Li et al. (2019). These models are denoted as SN-MMD-GAN-IKL, SN-SMMD-GAN-IKL and Rep-GAN-IKL. The results are reported in Table 1. As we can see, our KernelNet-based models obtain best results, showing the importance of data-dependent component.

In addition, the results on more models with different datasets are summarized in the Table 2, with the generated images shown in Figure 2 and Figure 3. Some results are taken from the corresponding papers, thus may not have standard deviations. We can see that our proposed method achieves competitive results on all the datasets, consistently improve different variants of MMD-GANs.

4.2 Implicit VAE

Multi-modal distribution sampling We first illustrate the implicit encoder can learn latent variable with multi-mode distributions. This is done by removing the decoder and only training the encoder, which essentially learns a

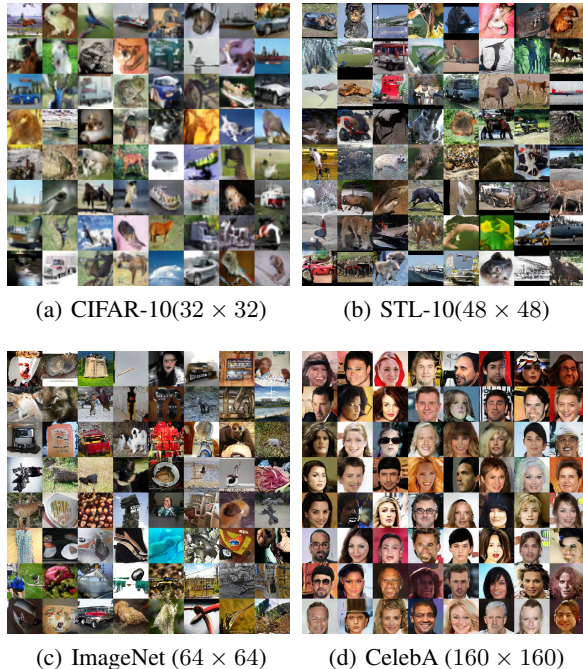


Figure 3: Generated images of Rep-GAN-DK.

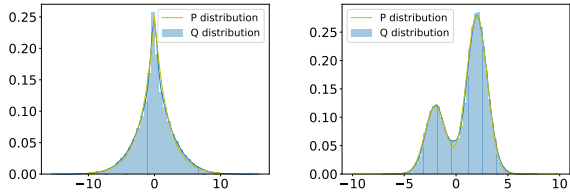


Figure 4: Learning to sample from two target distributions: Laplace(0, 2) (left) and Gaussian mixture $0.3\mathcal{N}(-2, 1) + 0.7\mathcal{N}(2, 1)$ (right). P -distribution denotes the ground truth; Q -distribution denotes the approximated density by samples.

parametric sampler. We use a 3-layer fully-connected neural network with 20 hidden units as the encoder, whose

Table 3: Negative log-likelihood on the binarized MNIST dataset.

MODEL	VAE	STEIN-VAE	SPECTRAL	SIVI	INFO-VAE	INFO-IVAE	INFO-IVAE-RBF	INFO-IVAE-IKL	INFO-IVAE-DK
NLL ↓	90.32	88.85	89.67	89.03	88.89	89.79	88.24	88.21	88.16

inputs are Gaussian noises. Figure 4 plots the learned distributions estimated by samples on two target distribution, which can perfectly generates multi-mode samples.

Implicit VAE Next, we test our Implicit Info-VAE model on the MNIST dataset (Salakhutdinov and Murray, 2008) to learn an implicit VAE model. We use a fully-connected neural network with 1 hidden layer for both encoder and decoder, whose hidden units are set to 400. ω_{ψ_1} and $\omega_{\psi_2, z_1, z_2}$ are parameterized by DNNs consisting of 2 fully connected hidden layers with 32 hidden units. Bernoulli noises are injected into the encoder by using dropout with a dropout rate of 0.3. The latent dimension is 32. The models are trained for 300 epochs. Stochastic gradient descent (SGD) with momentum of 0.9 is used with a batch size of 32. We sample 32 z for every x . The learning rate for the encoder and decoder is 0.002, while it is 0.001 for kernel learning. At every step, we sample 512 random features from the spectral distribution.

For fair evaluation, we follow Wu et al. (2016) and use Annealed Importance Sampling (AIS) to approximate the negative log-likelihood (NLL). 10 independent AIS chains are used, each of which have 1000 intermediate distributions. The final results are computed using 5000 random sampled test data. The results are shown in Table 3, where we compare with related models including: VAE (vanilla VAE from Kingma and Welling (2014)), Stein-VAE (amortized SVGD from Feng et al. (2017)), SIVI (Semi-Implicit VAE from Yin and Zhou (2018)), Spectral (implicit VAE with spectral method for gradient estimation from Shi et al. (2018)) and Info-VAE (Zhao et al., 2017).

We denote our Implicit Info-VAE with Stein gradient estimator with objective (1) as Info-IVAE. The models with objective (15) are denoted as Info-IVAE-RBF, Info-IVAE-IKL and Info-IVAE-DK, where the MMD regularizers are computed by RBF kernel, implicit kernel without data-dependent component and data-dependent KernelNet respectively.

Note that some models have also reported scores related to NLL in their original paper under different settings, which are not directly comparable to ours. For fair comparisons, we use the same encoder-decoder structure and rerun all the models. Our model obtains the best NLL score among all the models. Some reconstructed images and generated images of our model are shown in Figure 5.

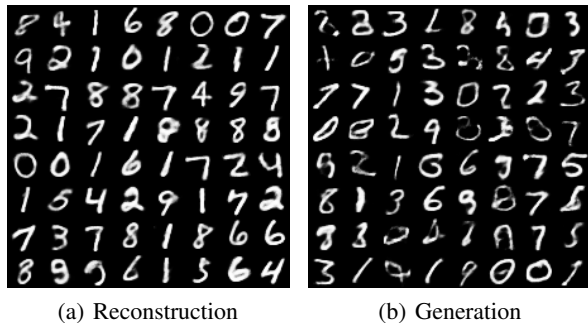


Figure 5: Reconstructed and generated images on MNIST.

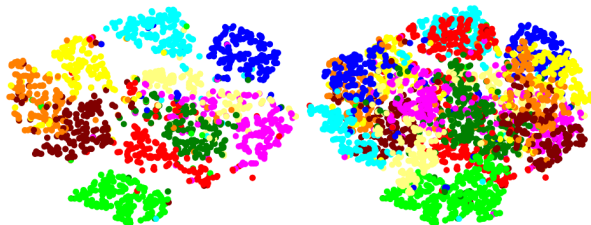


Figure 6: T-SNE visualization of learned latent variables on MNIST. Left and right figures correspond to the implicit kernel with/without data-dependent component, respectively.

We also plot the t -SNE visualization of latent variables learned by Info-IVAE-IK and Info-IVAE-DK in Figure 6. From the figure we can see that latent variables learned using data-dependent kernel looks more separable than implicit kernel without the data-dependent part. An extra semi-supervised experiment is also presented in Appendix D, where we follow Kingma et al. (2014) to evaluate the quality of the learned latent variables.

5 Conclusion

We propose KernelNet, a novel way of parameterizing learnable data-dependent kernels using implicit spectral distributions parameterized by DNNs. We prove existence of the data-dependent kernel, and present how the proposed KernelNet can be applied to deep generative models, including several variants of MMD-GAN and Info-VAE, along with some theoretical analysis. Experiments show that the proposed KernelNet leads to performance improvement over related models, demonstrating the effectiveness of data-dependent kernels.

References

- M. Arbel, D. J. Sutherland, M. Binkowski, and A. Gretton. On gradient regularizers for MMD gans. In *Advances in Neural Information Processing Systems 31: Annual Conference on Neural Information Processing Systems 2018, NeurIPS 2018, 3-8 December 2018, Montréal, Canada.*, pages 6701–6711, 2018.
- M. Arjovsky, S. Chintala, and L. Bottou. Wasserstein GAN. Technical Report arXiv:1701.07875, Mar. 2017.
- E. G. Bazavan, F. Li, and C. Sminchisescu. Fourier kernel learning. In *Computer Vision - ECCV 2012 - 12th European Conference on Computer Vision, Florence, Italy, October 7-13, 2012, Proceedings, Part II*, pages 459–473, 2012.
- W. Bounliphone, E. Belilovsky, M. B. Blaschko, I. Antonoglou, and A. Gretton. A test of relative similarity for model selection in generative models. In *4th International Conference on Learning Representations, ICLR 2016, San Juan, Puerto Rico, May 2-4, 2016, Conference Track Proceedings*, 2016.
- Y. Feng, D. Wang, and Q. Liu. Learning to draw samples with amortized stein variational gradient descent. In *UAI*, 2017.
- M. Gönen and E. Alpaydin. Multiple kernel learning algorithms. *Journal of Machine Learning Research*, 12:2211–2268, 2011. URL <http://dl.acm.org/citation.cfm?id=2021071>.
- I. Goodfellow, J. Pouget-Abadie, M. Mirza, B. Xu, D. Warde-Farley, S. Ozair, A. Courville, and Y. Bengio. Generative adversarial nets. In *Neural Information Processing Systems (NIPS)*, 2014.
- A. Gretton, K. M. Borgwardt, M. J. Rasch, B. Schölkopf, and A. J. Smola. A kernel two-sample test. *Journal of Machine Learning Research*, 13:723–773, 2012. URL <http://dl.acm.org/citation.cfm?id=2188410>.
- I. Gulrajani, F. Ahmed, M. Arjovsky, V. Dumoulin, and A. Courville. Improved training of Wasserstein GANs. In *NIPS*, 2017.
- M. Heusel, H. Ramsauer, T. Unterthiner, B. Nessler, G. Klambauer, and S. Hochreiter. Gans trained by a two time-scale update rule converge to a nash equilibrium. *CoRR*, abs/1706.08500, 2017. URL <http://arxiv.org/abs/1706.08500>.
- D. Kingma and J. Ba. Adam: A method for stochastic optimization. In *ICLR*, 2015.
- D. P. Kingma and M. Welling. Auto-encoding variational Bayes. In *ICLR*, 2014.
- D. P. Kingma, S. Mohamed, D. J. Rezende, and M. Welling. Semi-supervised learning with deep generative models. In *Advances in neural information processing systems*, pages 3581–3589, 2014.
- C. Li, W. Chang, Y. Cheng, Y. Yang, and B. Póczos. MMD GAN: towards deeper understanding of moment matching network. In *Advances in Neural Information Processing Systems 30: Annual Conference on Neural Information Processing Systems 2017, 4-9 December 2017, Long Beach, CA, USA*, pages 2200–2210, 2017.
- C.-L. Li, W.-C. Chang, Y. Mroueh, Y. Yang, and B. Póczos. Implicit kernel learning, 2019.
- Y. Li and R. E. Turner. Gradient estimators for implicit models. In *ICLR*, 2018.
- T. Miyato, T. Kataoka, M. Koyama, and Y. Yoshida. Spectral normalization for generative adversarial networks. In *6th International Conference on Learning Representations, ICLR 2018, Vancouver, BC, Canada, April 30 - May 3, 2018, Conference Track Proceedings*, 2018.
- C. S. Ong, X. Mary, S. Canu, and A. J. Smola. Learning with non-positive kernels. In *Proceedings of the twenty-first international conference on Machine learning*, page 81. ACM, 2004.
- A. Rahimi and B. Recht. Random features for large-scale kernel machines. In *NIPS*, 2007.
- D. J. Rezende, S. Mohamed, and D. Wierstra. Stochastic back-propagation and approximate inference in deep generative models. In *Proceedings of the 31st International Conference on Machine Learning*, pages 1278–1286, 2014.
- W. Rudin. *Fourier Analysis on Groups*. Wiley-Interscience, 1994.
- R. Salakhutdinov and I. Murray. On the quantitative analysis of deep belief networks. In *Machine Learning, Proceedings of the Twenty-Fifth International Conference (ICML 2008), Helsinki, Finland, June 5-9, 2008*, pages 872–879, 2008.
- T. Salimans, I. Goodfellow, W. Zaremba, V. Cheung, A. Radford, and X. Chen. Improved techniques for training GANs. In *NIPS*, 2016.
- B. Schölkopf and A. J. Smola. *Learning with Kernels: support vector machines, regularization, optimization, and beyond*. Adaptive computation and machine learning series. MIT Press, 2002. ISBN 9780262194754. URL <http://www.worldcat.org/oclc/48970254>.
- J. Shawe-Taylor and N. Cristianini. *Kernel Methods for Pattern Analysis*. Cambridge University Press, USA, 2004. ISBN 0521813972.
- J. Shi, S. Sun, and J. Zhu. A spectral approach to gradient estimation for implicit distributions. In *Proceedings of the 35th International Conference on Machine Learning*, pages 4651–4660, 2018.
- W. Wang, Y. Sun, and S. Halgamuge. Improving mmd-gan training with repulsive loss function, 2018.
- A. G. Wilson and R. P. Adams. Gaussian process kernels for pattern discovery and extrapolation. In *Proceedings of the 30th International Conference on Machine Learning, ICML 2013, Atlanta, GA, USA, 16-21 June 2013*, pages 1067–1075, 2013.
- Y. Wu, Y. Burda, R. Salakhutdinov, and R. B. Grosse. On the quantitative analysis of decoder-based generative models. *CoRR*, abs/1611.04273, 2016. URL <http://arxiv.org/abs/1611.04273>.
- M. Yin and M. Zhou. Semi-implicit variational inference. In *Proceedings of the 35th International Conference on Machine Learning, ICML 2018, Stockholm, Sweden, July 10-15, 2018*, pages 5646–5655, 2018.
- H. Zhang, Z. Zhang, A. Odena, and H. Lee. Consistency regularization for generative adversarial networks. In *International Conference on Learning Representations*, 2020. URL <https://openreview.net/forum?id=S1lxKlSKPH>.
- S. Zhao, J. Song, and S. Ermon. Infovae: Information maximizing variational autoencoders. *CoRR*, abs/1706.02262, 2017. URL <http://arxiv.org/abs/1706.02262>.

A Details on proposition 2

By Euler's formula, we have:

$$\kappa(\mathbf{z}_1, \mathbf{z}_2) = \int_{\mathbb{R}^d} p(\boldsymbol{\omega}) e^{j\boldsymbol{\omega}^\top(\mathbf{z}_1 - \mathbf{z}_2)} d\boldsymbol{\omega} = \mathbb{E}_{\boldsymbol{\omega}} \{ \cos[\boldsymbol{\omega}^\top(\mathbf{z}_1 - \mathbf{z}_2)] + j \sin[\boldsymbol{\omega}^\top(\mathbf{z}_1 - \mathbf{z}_2)] \}$$

For real-valued kernel, we remove the imaginary part, we have:

$$\kappa(\mathbf{z}_1, \mathbf{z}_2) = \mathbb{E}_{\boldsymbol{\omega}} \{ \cos[\boldsymbol{\omega}^\top(\mathbf{z}_1 - \mathbf{z}_2)] \}$$

Now we show $\mathbb{E}_{\boldsymbol{\omega}} \{ \cos[\boldsymbol{\omega}^\top(\mathbf{z}_1 - \mathbf{z}_2)] \} = 2\mathbb{E}_{\boldsymbol{\omega}, b} [\cos(\boldsymbol{\omega}^\top \mathbf{z}_1 + b) \cos(\boldsymbol{\omega}^\top \mathbf{z}_2 + b)]$, where b follows a uniform distribution $\mathcal{U}[0, 2\pi]$:

$$\begin{aligned} & 2\mathbb{E}_{\boldsymbol{\omega}, b} [\cos(\boldsymbol{\omega}^\top \mathbf{z}_1 + b) \cos(\boldsymbol{\omega}^\top \mathbf{z}_2 + b)] \\ &= 2\mathbb{E}_{\boldsymbol{\omega}} \mathbb{E}_b \{ [\cos(\boldsymbol{\omega}^\top \mathbf{z}_1) \cos b - \sin(\boldsymbol{\omega}^\top \mathbf{z}_1) \sin b] [\cos(\boldsymbol{\omega}^\top \mathbf{z}_2) \cos b - \sin(\boldsymbol{\omega}^\top \mathbf{z}_2) \sin b] \} \\ &= 2\mathbb{E}_{\boldsymbol{\omega}} \mathbb{E}_b (\cos \boldsymbol{\omega}^\top \mathbf{z}_1 \cos \boldsymbol{\omega}^\top \mathbf{z}_2 \cos^2 b - \sin \boldsymbol{\omega}^\top \mathbf{z}_1 \cos \boldsymbol{\omega}^\top \mathbf{z}_2 \sin b \cos b \\ &\quad - \cos \boldsymbol{\omega}^\top \mathbf{z}_1 \sin \boldsymbol{\omega}^\top \mathbf{z}_2 \sin b \cos b + \sin \boldsymbol{\omega}^\top \mathbf{z}_1 \sin \boldsymbol{\omega}^\top \mathbf{z}_2 \sin^2 b) \\ &= 2\mathbb{E}_{\boldsymbol{\omega}} \mathbb{E}_b [\cos \boldsymbol{\omega}^\top \mathbf{z}_1 \cos \boldsymbol{\omega}^\top \mathbf{z}_2 \cos^2 b + \sin \boldsymbol{\omega}^\top \mathbf{z}_1 \sin \boldsymbol{\omega}^\top \mathbf{z}_2 \sin^2 b] \\ &\quad - 2\mathbb{E}_{\boldsymbol{\omega}} \mathbb{E}_b [(\sin \boldsymbol{\omega}^\top \mathbf{z}_1 \cos \boldsymbol{\omega}^\top \mathbf{z}_2 - \cos \boldsymbol{\omega}^\top \mathbf{z}_1 \sin \boldsymbol{\omega}^\top \mathbf{z}_2) \sin^2 b] \\ &= 2\mathbb{E}_{\boldsymbol{\omega}} \mathbb{E}_b [\cos \boldsymbol{\omega}^\top \mathbf{z}_1 \cos \boldsymbol{\omega}^\top \mathbf{z}_2 \cos^2 b + \sin \boldsymbol{\omega}^\top \mathbf{z}_1 \sin \boldsymbol{\omega}^\top \mathbf{z}_2 \sin^2 b] \\ &= 2\mathbb{E}_{\boldsymbol{\omega}} \{ \cos \boldsymbol{\omega}^\top \mathbf{z}_1 \cos \boldsymbol{\omega}^\top \mathbf{z}_2 \mathbb{E}_b (\cos 2b + 1) + \sin \boldsymbol{\omega}^\top \mathbf{z}_1 \sin \boldsymbol{\omega}^\top \mathbf{z}_2 \mathbb{E}_b (1 - \cos 2b) \} \\ &= \mathbb{E}_{\boldsymbol{\omega}} [(\cos \boldsymbol{\omega}^\top \mathbf{z}_1 \cos \boldsymbol{\omega}^\top \mathbf{z}_2 + \sin \boldsymbol{\omega}^\top \mathbf{z}_1 \sin \boldsymbol{\omega}^\top \mathbf{z}_2) \mathbb{E}_b (1)] \\ &= \mathbb{E}_{\boldsymbol{\omega}} (\cos \boldsymbol{\omega}^\top \mathbf{z}_1 \cos \boldsymbol{\omega}^\top \mathbf{z}_2 + \sin \boldsymbol{\omega}^\top \mathbf{z}_1 \sin \boldsymbol{\omega}^\top \mathbf{z}_2) \\ &= \mathbb{E}_{\boldsymbol{\omega}} \{ \cos[\boldsymbol{\omega}^\top(\mathbf{z}_1 - \mathbf{z}_2)] \} \end{aligned}$$

The proposition has been proved.

B Proof of proposition 4

We start from the following Lemma:

Lemma 6 ((Arbel et al., 2018)) Assume the critic functions, which have form:

$$f_{\nu}(\mathbf{a}) = (\mathbb{E}_{\mathbf{x} \sim \mathbb{P}} k_{\nu}(\mathbf{x}, \mathbf{a}) - \mathbb{E}_{\mathbf{y} \sim \mathbb{Q}} k_{\nu}(\mathbf{y}, \mathbf{a})) / \text{MMD}_{k_{\nu}}(\mathbb{P}, \mathbb{Q})$$

are uniformly bounded and have a common Lipschitz constant:

$$\sup_{\mathbf{a} \in \mathbb{R}^D, \nu \in \mathcal{V}} |f_{\nu}(\mathbf{a})| < \infty \quad \sup_{\nu \in \mathcal{V}} \|f_{\nu}(\mathbf{a})\|_{Lip} < \infty.$$

Then $\text{MMD}_{k_{\nu}}(\mathbb{P}, \mathbb{Q})$ is continuous in the weak topology. In particular, this holds when $k_{\nu} = \kappa \circ h_{\phi}$ and

$$\sup_{\mathbf{z} \in \mathbb{R}^d} \kappa(\mathbf{z}, \mathbf{z}) < \infty, \quad \|\kappa(\mathbf{z}_1, \cdot) - \kappa(\mathbf{z}_2, \cdot)\|_{\mathcal{H}_{\kappa}} \leq L_{\kappa} \|\mathbf{z}_1 - \mathbf{z}_2\|_{\mathbb{R}^d}, \quad \sup_{\phi \in \Phi} \|h_{\phi}\|_{Lip} < \infty$$

From (2) we know that $\sup_{\mathbf{z}_1 \in \mathbb{R}^d} \kappa_{\psi}(\mathbf{z}_1, \mathbf{z}_1) < \infty$ is naturally satisfied. We prove the second condition in Lemma 6 here:

$$\begin{aligned}
& \|\kappa_{\psi}(\mathbf{z}_1, \cdot) - \kappa_{\psi}(\mathbf{z}_2, \cdot)\|_{\mathcal{H}} \\
& \leq \sqrt{\langle \kappa_{\psi}(\mathbf{z}_1, \cdot) - \kappa_{\psi}(\mathbf{z}_2, \cdot), \kappa_{\psi}(\mathbf{z}_1, \cdot) - \kappa_{\psi}(\mathbf{z}_2, \cdot) \rangle_{\mathcal{H}}} \\
& = \sqrt{\kappa_{\psi}(\mathbf{z}_1, \mathbf{z}_1) + \kappa_{\psi}(\mathbf{z}_2, \mathbf{z}_2) - 2\kappa_{\psi}(\mathbf{z}_1, \mathbf{z}_2)} \\
& = \sqrt{\kappa_{\psi_1}(\mathbf{z}_1, \mathbf{z}_1) + \kappa_{\psi_1}(\mathbf{z}_2, \mathbf{z}_2) - 2\kappa_{\psi_1}(\mathbf{z}_1, \mathbf{z}_2) + \kappa_{\psi_2}(\mathbf{z}_1, \mathbf{z}_1) + \kappa_{\psi_2}(\mathbf{z}_2, \mathbf{z}_2) - 2\kappa_{\psi_2}(\mathbf{z}_1, \mathbf{z}_2)} \\
& \leq \sqrt{2 - 2\kappa_{\psi_1}(\mathbf{z}_1, \mathbf{z}_2)} + \sqrt{2 - 2\kappa_{\psi_2}(\mathbf{z}_1, \mathbf{z}_2)} \tag{16}
\end{aligned}$$

Let start with the second term above, denote $f_2(\mathbf{t}) = 2 - \kappa_2(\mathbf{t})$, where $\mathbf{t} = \mathbf{z}_1 - \mathbf{z}_2$.

$$\begin{aligned}
& \|\nabla_{\mathbf{t}} f_2(\mathbf{t})\| \\
& = \|\nabla_{\mathbf{t}} [2 - 2\kappa_{\psi_2}(\mathbf{t})]\| \\
& = \|\nabla_{\mathbf{t}} \{2 - 2\mathbb{E}_{\omega_{\psi_2, \mathbf{t}}} [\cos(\omega_{\psi_2, \mathbf{t}}^{\top} \mathbf{t})]\}\| \\
& = 2\|\mathbb{E}_{\omega_{\psi_2, \mathbf{t}}} [\sin(\omega_{\psi_2, \mathbf{t}}^{\top} \mathbf{t}) (\omega_{\psi_2, \mathbf{t}}^{\top} \mathbf{t} + \mathbf{t} \nabla_{\mathbf{t}} \omega_{\psi_2, \mathbf{t}})]\| \\
& \leq 2\|\mathbb{E}_{\omega_{\psi_2, \mathbf{t}}} [\sin(\omega_{\psi_2, \mathbf{t}}^{\top} \mathbf{t}) \omega_{\psi_2, \mathbf{t}}]\| + 2\|\mathbb{E}_{\omega_{\psi_2, \mathbf{t}}} [\sin(\omega_{\psi_2, \mathbf{t}}^{\top} \mathbf{t}) \mathbf{t} \nabla_{\mathbf{t}} \omega_{\psi_2, \mathbf{t}}]\| \\
& \leq 2\mathbb{E}_{\omega_{\psi_2, \mathbf{t}}} (\|\mathbf{t}\| \|\omega_{\psi_2, \mathbf{t}}\|^2) + 2\mathbb{E}_{\omega_{\psi_2, \mathbf{t}}} (\|\mathbf{t}\| \|\nabla_{\mathbf{t}} \omega_{\psi_2, \mathbf{t}}\|_{\mathcal{F}}) \\
& = 2\mathbb{E}_{\omega_{\psi_2, \mathbf{t}}} [\|\mathbf{t}\| (\|\omega_{\psi_2, \mathbf{t}}\|^2 + \|\nabla_{\mathbf{t}} \omega_{\psi_2, \mathbf{t}}\|_{\mathcal{F}})]
\end{aligned}$$

If $2\mathbb{E}_{\omega_{\psi_2, \mathbf{t}}} [\|\omega_{\psi_2, \mathbf{t}}\|^2] \leq c_1$ and $2\mathbb{E}_{\omega_{\psi_2, \mathbf{t}}} [\|\nabla_{\mathbf{t}} \omega_{\psi_2, \mathbf{t}}\|_{\mathcal{F}}] \leq c_2$, for constants c_1, c_2 , then we have $\|\nabla_{\mathbf{t}} f_2(\mathbf{t})\| \leq c\|\mathbf{t}\|$, where $c = c_1 + c_2$.

$$\begin{aligned}
\|f_2(\mathbf{t})\| & = \left\| \int \nabla_{\mathbf{t}} f_2(\mathbf{t}) d\mathbf{t} \right\| = \int \|\nabla_{\mathbf{t}} f_2(\mathbf{t})\| d\mathbf{t} \\
& \leq c \int \|\mathbf{t}\| d\mathbf{t} = c \int \sqrt{\sum_{i=1}^d t_i^2} d\mathbf{t} \\
& \leq c \sum_{i=1}^d \int |t_i| d\mathbf{t}_i \\
& \leq c \sum_{i=1}^d \frac{t_i^2}{2} = \frac{c}{2} \|\mathbf{t}\|^2
\end{aligned}$$

Thus we can conclude, if

$$\mathbb{E}_{\omega_{\psi_2, \mathbf{t}}} [\|\omega_{\psi_2, \mathbf{t}}\|^2] < \infty, \quad \mathbb{E}_{\omega_{\psi_2, \mathbf{t}}} [\|\nabla_{\mathbf{t}} \omega_{\psi_2, \mathbf{t}}\|_{\mathcal{F}}] < \infty$$

then $\sqrt{f_2(\mathbf{t})} \leq \sqrt{\frac{c}{2}} \|\mathbf{t}\|$ holds. Similar result can be easily get for the first term in (16). Then we can conclude if:

$$\mathbb{E}_{\omega_{\psi_1}} [\|\omega_{\psi_1}\|^2] < \infty, \quad \mathbb{E}_{\omega_{\psi_2, \mathbf{t}}} [\|\omega_{\psi_2, \mathbf{t}}\|^2] < \infty, \quad \mathbb{E}_{\omega_{\psi_2, \mathbf{t}}} [\|\nabla_{\mathbf{t}} \omega_{\psi_2, \mathbf{t}}\|_{\mathcal{F}}] < \infty \tag{17}$$

then

$$\|\kappa_{\psi}(\mathbf{z}_1, \cdot) - \kappa_{\psi}(\mathbf{z}_2, \cdot)\|_{\mathcal{H}} \leq L_{\kappa} \|\mathbf{t}\| = L_{\kappa} \|\mathbf{z}_1 - \mathbf{z}_2\|$$

For some constant L_{κ} . Because $\mathbf{t} = \mathbf{z}_1 - \mathbf{z}_2$, we have:

$$\nabla_{\mathbf{t}} \omega_{\psi_2, \mathbf{t}} = \frac{\partial \omega_{\psi_2, \mathbf{z}_1, \mathbf{z}_2}}{\partial \mathbf{z}_1} \frac{\partial \mathbf{z}_1}{\partial \mathbf{t}} + \frac{\partial \omega_{\psi_2, \mathbf{z}_1, \mathbf{z}_2}}{\partial \mathbf{z}_2} \frac{\partial \mathbf{z}_2}{\partial \mathbf{t}} = \frac{\partial \omega_{\psi_2, \mathbf{z}_1, \mathbf{z}_2}}{\partial \mathbf{z}_1} - \frac{\partial \omega_{\psi_2, \mathbf{z}_1, \mathbf{z}_2}}{\partial \mathbf{z}_2} \tag{18}$$

Substitute (18) into (17), proposition 4 is proved.

C Details on proposition 5

In our data-dependent kernel setting, $k = \kappa_{\psi} \circ h_{\phi}$, hence we write $k(\mathbf{y}, \mathbf{z}) = \kappa_{\psi}(h_{\phi}(\mathbf{y}), h_{\phi}(\mathbf{z}))$, where h_{ϕ} is the discriminator, and κ_{ψ} is the proposed data-dependent kernel. For our data-dependent kernel, we know that

$$\int \kappa_{\psi, \phi}(\mathbf{x}, \mathbf{x}) d\mathbb{P}(\mathbf{x}) = 1$$

from (2).

$$\begin{aligned} & \sum_{i=1}^d \int \frac{\partial^2 \kappa_{\psi}(\mathbf{y}_1, \mathbf{y}_2)}{\partial \mathbf{y}_{1i} \partial \mathbf{y}_{2i}} \Big|_{(\mathbf{y}_1, \mathbf{y}_2) = (\mathbf{x}, \mathbf{x})} d\mathbb{P}(\mathbf{x}) \\ &= \sum_{i=1}^d \int \frac{\partial^2 \kappa_{\psi_1}(\mathbf{y}_1, \mathbf{y}_2)}{\partial \mathbf{y}_{1i} \partial \mathbf{y}_{2i}} \Big|_{(\mathbf{y}_1, \mathbf{y}_2) = (\mathbf{x}, \mathbf{x})} d\mathbb{P}(\mathbf{x}) + \sum_{i=1}^d \int \frac{\partial^2 \kappa_{\psi_2}(\mathbf{y}_1, \mathbf{y}_2)}{\partial \mathbf{y}_{1i} \partial \mathbf{y}_{2i}} \Big|_{(\mathbf{y}_1, \mathbf{y}_2) = (\mathbf{x}, \mathbf{x})} d\mathbb{P}(\mathbf{x}) \end{aligned}$$

where $\mathbf{z}_1 = h_{\phi}(\mathbf{y}_1)$ and $\mathbf{z}_2 = h_{\phi}(\mathbf{y}_2)$. For clearness, we will write $\boldsymbol{\omega}_{\psi_2}$ instead of $\boldsymbol{\omega}_{\psi_2, \mathbf{z}_1, \mathbf{z}_2}$, but please keep in mind that $\boldsymbol{\omega}_{\psi_2}$ is dependent on the input data. Because of the reparameterization trick, we can write $\mathbb{E}_{\epsilon \sim \mathcal{N}(\mathbf{0}, \mathbf{I})}(\cdot)$ instead of $\mathbb{E}_{\boldsymbol{\omega}_{\psi_2, \mathbf{z}_1, \mathbf{z}_2}}(\cdot)$,

$$\begin{aligned} & \sum_{i=1}^d \int \frac{\partial^2 \kappa_{\psi_2}(\mathbf{y}_1, \mathbf{y}_2)}{\partial \mathbf{y}_{1i} \partial \mathbf{y}_{2i}} \Big|_{(\mathbf{y}_1, \mathbf{y}_2) = (\mathbf{x}, \mathbf{x})} d\mathbb{P}(\mathbf{x}) \\ &= \sum_{i=1}^d \int \frac{\partial^2 \mathbb{E}_{\epsilon \sim \mathcal{N}(\mathbf{0}, \mathbf{I})} \{ \cos \{ \boldsymbol{\omega}_{\psi_2}^{\top} [h_{\phi}(\mathbf{y}_1) - h_{\phi}(\mathbf{y}_2)] \} \}}{\partial \mathbf{y}_{1i} \partial \mathbf{y}_{2i}} \Big|_{(\mathbf{y}_1, \mathbf{y}_2) = (\mathbf{x}, \mathbf{x})} d\mathbb{P}(\mathbf{x}) \\ &= \sum_{i=1}^d \int \int \frac{\partial}{\partial \mathbf{y}_{2i}} \sin \{ \boldsymbol{\omega}_{\psi_2}^{\top} [h_{\phi}(\mathbf{y}_1) - h_{\phi}(\mathbf{y}_2)] \} \\ & \quad \left\{ \frac{\partial \boldsymbol{\omega}_{\psi_2}^{\top}}{\partial \mathbf{y}_{1i}} [h_{\phi}(\mathbf{y}_1) - h_{\phi}(\mathbf{y}_2)] + \boldsymbol{\omega}_{\psi_2}^{\top} \frac{\partial h_{\phi}(\mathbf{y}_1)}{\partial \mathbf{y}_{1i}} \right\} d\boldsymbol{\mu}(\boldsymbol{\epsilon}) \Big|_{(\mathbf{y}_1, \mathbf{y}_2) = (\mathbf{x}, \mathbf{x})} d\mathbb{P}(\mathbf{x}) \\ &= \sum_{i=1}^d \int \int -\cos \{ \boldsymbol{\omega}_{\psi_2}^{\top} [h_{\phi}(\mathbf{y}_1) - h_{\phi}(\mathbf{y}_2)] \} \left\{ \frac{\partial \boldsymbol{\omega}_{\psi_2}^{\top}}{\partial \mathbf{y}_{2i}} [h_{\phi}(\mathbf{y}_1) - h_{\phi}(\mathbf{y}_2)] + \boldsymbol{\omega}_{\psi_2}^{\top} \left[-\frac{\partial h_{\phi}(\mathbf{y}_2)}{\partial \mathbf{y}_{2i}} \right] \right\} \\ & \quad \times \left\{ \frac{\partial \boldsymbol{\omega}_{\psi_2}^{\top}}{\partial \mathbf{y}_{1i}} [h_{\phi}(\mathbf{y}_1) - h_{\phi}(\mathbf{y}_2)] + \boldsymbol{\omega}_{\psi_2}^{\top} \frac{\partial h_{\phi}(\mathbf{y}_1)}{\partial \mathbf{y}_{1i}} \right\} \\ & \quad + \sin \{ \boldsymbol{\omega}_{\psi_2}^{\top} [h_{\phi}(\mathbf{y}_1) - h_{\phi}(\mathbf{y}_2)] \} \frac{\partial}{\partial \mathbf{y}_{2i}} \left\{ \frac{\boldsymbol{\omega}_{\psi_2}^{\top}}{\partial \mathbf{y}_{1i}} [h_{\phi}(\mathbf{y}_1) - h_{\phi}(\mathbf{y}_2)] + \boldsymbol{\omega}_{\psi_2}^{\top} \frac{\partial h_{\phi}(\mathbf{y}_1)}{\partial \mathbf{y}_{1i}} \right\} d\boldsymbol{\mu}(\boldsymbol{\epsilon}) \Big|_{(\mathbf{y}_1, \mathbf{y}_2) = (\mathbf{x}, \mathbf{x})} d\mathbb{P}(\mathbf{x}) \\ &= \sum_{i=1}^d \int \int \left[\boldsymbol{\omega}_{\psi_2, \mathbf{z}, \mathbf{z}}^{\top} \frac{\partial h_{\phi}(\mathbf{x})}{\partial \mathbf{x}_i} \right]^2 d\boldsymbol{\mu}(\boldsymbol{\epsilon}) d\mathbb{P}(\mathbf{x}) \end{aligned}$$

where $\mathbf{z} = h_{\phi}(\mathbf{x})$. In our experiment, the output dimension of discriminator h_{ϕ} is set to be 1. Then the result becomes:

$$\sum_{i=1}^d \int \frac{\partial^2 \kappa_{\boldsymbol{\omega}_{\psi_2, \mathbf{z}_1, \mathbf{z}_2}}(\mathbf{y}_1, \mathbf{y}_2)}{\partial \mathbf{y}_{1i} \partial \mathbf{y}_{2i}} \Big|_{(\mathbf{y}_1, \mathbf{y}_2) = (\mathbf{x}, \mathbf{x})} d\mathbb{P}(\mathbf{x}) = \mathbb{E}_{\mathbf{x} \sim \mathbb{P}} \{ \mathbb{E}_{\boldsymbol{\omega}_{\psi_2, \mathbf{z}, \mathbf{z}}} [\|\boldsymbol{\omega}_{\psi_2, \mathbf{z}, \mathbf{z}}\|^2] \|\nabla h_{\phi}(\mathbf{x})\|_{\mathcal{F}} \}$$

Similarly, we have:

$$\sum_{i=1}^d \int \frac{\partial^2 \kappa_{\boldsymbol{\omega}_{\psi_1}}(\mathbf{y}_1, \mathbf{y}_2)}{\partial \mathbf{y}_{1i} \partial \mathbf{y}_{2i}} \Big|_{(\mathbf{y}_1, \mathbf{y}_2) = (\mathbf{x}, \mathbf{x})} d\mathbb{P}(\mathbf{x}) = \mathbb{E}_{\mathbf{x} \sim \mathbb{P}} \{ \mathbb{E}_{\boldsymbol{\omega}_{\psi_1}} [\|\boldsymbol{\omega}_{\psi_1}\|^2] \|\nabla h_{\phi}(\mathbf{x})\|_{\mathcal{F}} \}$$

Hence:

$$\begin{aligned} & \sum_{i=1}^d \int \frac{\partial^2 \kappa_{\omega}(\mathbf{y}_1, \mathbf{y}_2)}{\partial \mathbf{y}_{1i} \partial \mathbf{y}_{2i}} \Big|_{(\mathbf{y}_1, \mathbf{y}_2) = (\mathbf{x}, \mathbf{x})} d\mathbb{P}(\mathbf{x}) \\ &= \mathbb{E}_{\mathbf{x} \sim \mathbb{P}} \{ \mathbb{E}_{\omega_{\psi_2, \mathbf{z}, \mathbf{z}}} [\|\omega_{\psi_2, \mathbf{z}, \mathbf{z}}\|^2] + \mathbb{E}_{\omega_{\psi_1}} [\|\omega_{\psi_1}\|^2] \} \|\nabla h_{\phi}(\mathbf{x})\|_{\mathcal{F}} \end{aligned} \quad (19)$$

D Extra Experiments

We evaluate the latent variables learned by Info-IVAE with different kernels following Kingma et al. (2014). After we finish training Info-IVAE models, we generate latent features using the encoders. Then we train a SVM on these latent features. More informative latent variables should lead to better classification performance, the results are shown in Figure 7.

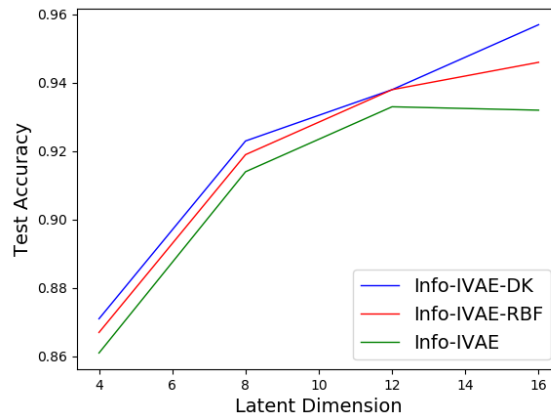


Figure 7: Semi-supervised experiment on Mnist dataset